



Flat-band full localization and symmetry-protected topological phase on bilayer lattice systemsIkuo Ichinose *Department of Applied Physics, Nagoya Institute of Technology, Nagoya 466-8555, Japan*Takahiro Orito *Quantum Matter Program, Graduate School of Advanced Science and Engineering, Hiroshima University, Higashi-Hiroshima 739-8530, Japan*Yoshihito Kuno *Department of Physics, Graduate School of Science, Tsukuba University, Tsukuba, Ibaraki 305-8571, Japan*

(Received 26 February 2021; accepted 14 May 2021; published 27 May 2021)

In this work, we present bilayer flat-band Hamiltonians, in which all bulk states are localized and specified by extensive local integrals of motion (LIOMs). The present systems are bilayer extension of the Creutz ladder, which is studied previously. In order to construct models, we employ building blocks, cube operators, which are linear combinations of fermions defined in each cube of the bilayer lattice. There are eight cubic operators, and the Hamiltonians are composed of the number operators of them, the LIOMs. A suitable arrangement of locations of the cube operators is needed to have exact projective Hamiltonians. The projective Hamiltonians belong to a topological classification class, the BDI class. With the open boundary condition, the constructed Hamiltonians have gapless edge modes, which commute with each other as well as the Hamiltonian. This result comes from a symmetry analogous to the one-dimensional chiral symmetry of the BDI class. These results indicate that the projective Hamiltonians describe a kind of symmetry-protected topological phase matter. Careful investigation of topological indexes, such as the Berry phase and string operator, is given. We also show that, by using the gapless edge modes, a generalized Sachdev-Ye-Kitaev model is constructed.

DOI: [10.1103/PhysRevB.103.184113](https://doi.org/10.1103/PhysRevB.103.184113)**I. INTRODUCTION**

Flat-band systems are one of the most attractive topics in the condensed matter community. Such systems exhibit exotic localization phenomena without disorder, currently called disorder-free localization [1–5]. In particular, the system, which is totally composed of flat bands and called a complete flat-band system, generally possesses an extensive number of local conserved quantities called local integrals of motion (LIOMs) [6–9]. Without interactions, complete flat-band systems are, therefore, integrable and their dynamics exhibits nonthermalized behaviors [10–12]. The idea of LIOMs was first introduced in the study of many-body localization (MBL) [6–9]. There, emergent LIOMs induce localization, a nonthermalized dynamics with slow increase of entanglement entropy [13]. On the other hand, in the complete flat-band systems, the origin of the LIOMs is due to the presence of the compact localized states (CLSs) [14–17]; hence the LIOMs are explicitly given in terms of the number operator of the CLSs. The origin of LIOMs in these systems is essentially different from that of the emergent LIOMs in the MBL systems, but both of them play an important role concerning localization.

From another point of view, flat-band systems with nontrivial topological bands have attracted much interest. On flat bands, the kinetic terms are negligible and interactions play a dominant role in determining the ground state. Then, such a system possibly exhibits exotic topological phases. The fractional Chern insulator is expected to be realized in nearly

flat-band systems [18,19], and for complete flat-band systems, fractional topological phenomena have been reported [20–22]. Also, flat-band systems are closely related to frustrated systems, in which huge degeneracies exist in the vicinity of the ground state, and as a result, some kinds of topological phases possibly emerge there [23–26]. Recently, some interesting works on flat-band systems with nontrivial topological bands have been reported [27–29].

As a typical example of such a flat-band system, the Creutz ladder [30] with a fine-tuning is an interesting system, where the two complete flat bands and the two types of CLSs appear. Due to the presence of the extensive number of CLSs, the model exhibits explicitly disorder-free localization phenomena, called Aharonov-Bohm caging [10–12]. It is known that localization tendency survives even in the presence of interactions [31–35]. Furthermore, the Creutz ladder shows some topological phases with quantized Berry phase and zero energy edge states [30,36–40], and interestingly fractional topological phenomena [22]. However, except for the Creutz ladder, complete flat-band models with nontrivial topological properties have not been studied in great detail so far. Hence, exploring such a model that goes beyond the above example remains an open issue.

In the present paper, by extending the character of the CLS in the Creutz ladder, we propose types of flat-band systems on a bilayer lattice, which can be set in both one- (1D) and two-dimensional (2D) lattice geometries. There, the extensive

LIOMs are explicitly obtained and all states are localized in the periodic boundary condition. As a topological aspect, the system Hamiltonians have symmetries of the BDI class in a *tenfold way* [41–44]. With BDI symmetry, the system Hamiltonian set on a quasi-1D lattice explicitly exhibits a symmetry protected topological (SPT) phase [45–47]. Also, we find that, in both 1D and 2D systems with open boundary conditions, there emerge gapless edge modes as a result of chiral symmetry. The gapless edge modes can be analytically given due to the presence of the CLS. Therefore, the presence of the edge modes implies that the present systems can be regarded as a 2D SPT system whose bulk states are full localized. Such kinds of models in one dimension are studied, e.g., in Ref. [48].

This paper is organized as follows. In Sec. II, we prepare building blocks called cube operators that are used for the construction of the model Hamiltonians. There are eight kinds of cube operators, which are linear combinations of fermions located on eight sites of a cube. The cube operators located on the same cube commute with each other, but certain pairs of them located on next-nearest-neighbor (NNN) cubes do not. The cube operators transform with each other by chiral-symmetry transformation, and we require the invariance of the Hamiltonian under chiral-symmetry transformation. In Sec. III, we construct models and their Hamiltonian by using the cube operators. A certain specific location of eight kinds of the cube operators is required to obtain the exact projective Hamiltonian. We present two kinds of such Hamiltonians, one of which is defined on a bilayer lattice and the other on a square prism lattice. Interactions between fermions can be introduced, which are expressed by the LIOMs and satisfy chiral symmetry. Section IV is devoted to study of the edge modes in the above two models. As a result of chiral symmetry of the bulk Hamiltonian, the edge modes are invariant under the transformation corresponding to chiral symmetry. Furthermore, the effective Hamiltonian of the edge modes is derived, which is an extension of the Sachdev-Ye-Kitaev (SYK) model [49–51]. Section V is devoted to discussion of topological indices, which characterize nontrivial topological properties of the emergent eigenstates. Numerical study of the square prism model is given to examine the stability of the topological states. Section VI is devoted to conclusion and discussion. We explain that flat-band localization by the CLS plays an important role for topological properties of the systems.

II. CONSTRUCTION OF BILAYER MODELS

In previous works [33–35], we studied fermion systems on the Creutz ladder, and obtained interesting results concerning flat-band localization and topological phase. In this section, we construct fermion systems on the bilayer lattice that exhibits the full-localization and topological properties. These systems have projective Hamiltonians with time-reversal (\mathcal{T}), particle-hole (\mathcal{C}), and chiral symmetries ($\mathcal{S} = \mathcal{TC}$). As a result, they have gapless edge modes under the open boundary condition (OBC), whereas the bulk states are fully localized and have flat-band dispersion. To construct models, we prepare eight building blocks with the cubic shape, each edge of which corresponds to a linear combination of fermions at

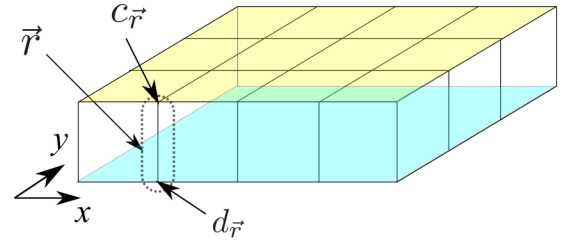


FIG. 1. Schematic picture of fermion operators on the bilayer lattice. $c_{\vec{r}}$'s reside on the upper square lattice, and $d_{\vec{r}}$'s on the lower lattice, where $\vec{r} = (x, y)$.

two sites of the edge, which is an extension of the CLS in the Creutz ladder [30,36,37,39]. Using these building blocks, called cube operators, we can construct bilayer models with various shapes, including a torus, a thin cylinder, and a square prism. In the context of the study of MBL, each cube operator is also regarded as an ℓ -bit (equivalent to the CLS) [14], and the target Hamiltonians are obtained by using LIOMs, which are nothing but the number operator of the ℓ -bits (CLS).

A. Eight cube operators

Let us consider a cube, which is a unit cell of the bilayer lattice; i.e., each vertex of the cube is located at a lattice site (see Fig. 1). We introduce $(x$ - y - $z)$ axes, and fermion creation (annihilation) operators $c_{\vec{r}}^{\dagger}$ ($c_{\vec{r}}$) and $d_{\vec{r}}^{\dagger}$ ($d_{\vec{r}}$), where \vec{r} denotes lattice sites, $\vec{r} = (x, y, z)$, and $z = 1$ (2) for $c_{\vec{r}}$ ($d_{\vec{r}}$). Therefore, the fermion $c_{\vec{r}}$ and $d_{\vec{r}}$ are located in the upper and lower layer, respectively, and then we use $\vec{r} = (x, y)$ hereafter.

The eight cube operators are constructed by $c_{\vec{r}}$ and $d_{\vec{r}}$. To this end, as elementary building blocks, the following notations are useful:

$$\begin{aligned} \omega_{\vec{r},\hat{i}}^A &= c_{\vec{r}+\hat{i}} + ic_{\vec{r}}, & \omega_{\vec{r},\hat{i}}^B &= c_{\vec{r}+\hat{i}} - ic_{\vec{r}} & (\text{upper layer}), \\ \tilde{\omega}_{\vec{r},\hat{i}}^A &= d_{\vec{r}+\hat{i}} + id_{\vec{r}}, & \tilde{\omega}_{\vec{r},\hat{i}}^B &= d_{\vec{r}+\hat{i}} - id_{\vec{r}} & (\text{lower layer}), \\ \bar{\omega}_{\vec{r},\hat{z}}^A &= c_{\vec{r}} + id_{\vec{r}}, & \bar{\omega}_{\vec{r},\hat{z}}^B &= c_{\vec{r}} - id_{\vec{r}} & (\text{interlayer}), \end{aligned} \quad (1)$$

where $\hat{i} = \hat{x}, \hat{y}$. It is easily verified:

$$\{\omega_{\vec{r},\hat{i}}^A, \omega_{\vec{r},\hat{j}}^B\} = 0,$$

etc. By using the above notation in Eq. (1), the eight cube operators are schematically displayed in Fig. 2. It should be remarked that it is not obvious if configurations of ω^A , $\tilde{\omega}^A$, etc. shown in Fig. 2 can be constructed consistently. We give explicit forms of the cube operators corresponding to those in Fig. 2:

$$\begin{aligned} Q_{\vec{r}}^+ &= \frac{1}{\sqrt{8}}[-d_{\vec{r}+\hat{x}+\hat{y}} + id_{\vec{r}+\hat{x}} + id_{\vec{r}+\hat{y}} - d_{\vec{r}} \\ &\quad - ic_{\vec{r}+\hat{x}+\hat{y}} + c_{\vec{r}+\hat{x}} + c_{\vec{r}+\hat{y}} - ic_{\vec{r}}], \\ Q_{\vec{r}}^- &= \frac{1}{\sqrt{8}}[-d_{\vec{r}+\hat{x}+\hat{y}} + id_{\vec{r}+\hat{x}} - id_{\vec{r}+\hat{y}} + d_{\vec{r}} \\ &\quad - ic_{\vec{r}+\hat{x}+\hat{y}} + c_{\vec{r}+\hat{x}} - c_{\vec{r}+\hat{y}} + ic_{\vec{r}}], \\ \tilde{Q}_{\vec{r}}^+ &= \frac{1}{\sqrt{8}}[d_{\vec{r}+\hat{x}+\hat{y}} - id_{\vec{r}+\hat{x}} - id_{\vec{r}+\hat{y}} + d_{\vec{r}} \\ &\quad - ic_{\vec{r}+\hat{x}+\hat{y}} + c_{\vec{r}+\hat{x}} + c_{\vec{r}+\hat{y}} - ic_{\vec{r}}], \end{aligned}$$

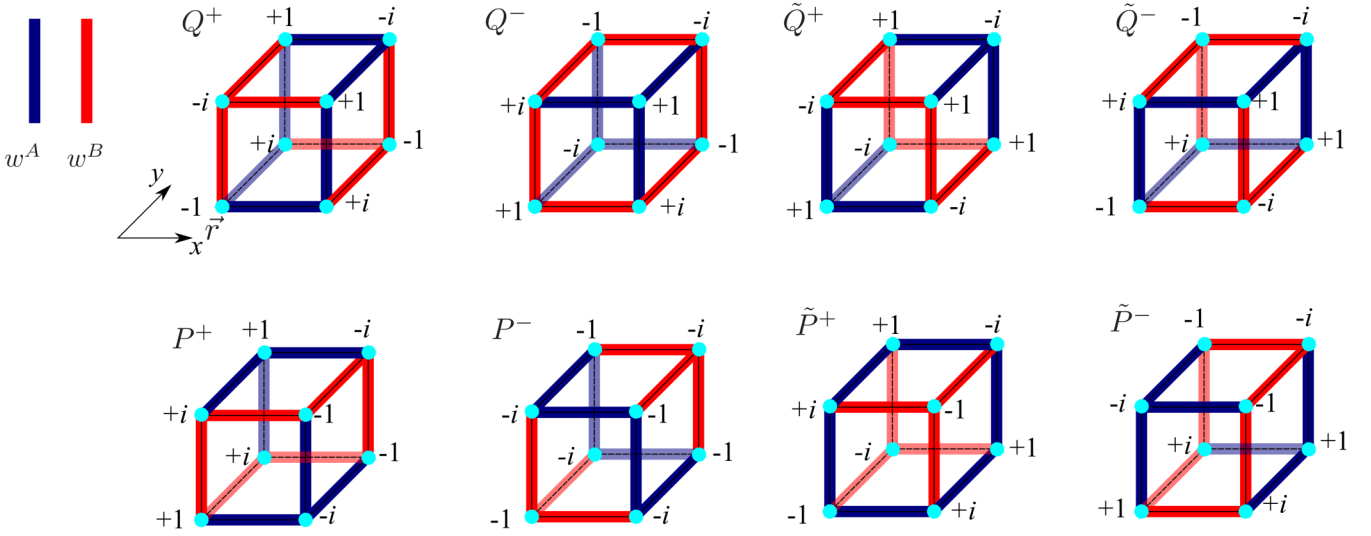


FIG. 2. Schematic picture of eight cube operators on the bilayer lattice, Q_r^+ through \tilde{P}_r^- . The eight cube operators are linear combinations of $\{\omega_{r,i}^A, \tilde{\omega}_{r,i}^A, \tilde{\omega}_{r,i}^{A-}$ (blue) and $\{\omega_{r,i}^B, \tilde{\omega}_{r,i}^B, \tilde{\omega}_{r,i}^{B-}$ (red). The numbers near vertices of the cube indicate the value of the coefficient of the cube operators.

$$\begin{aligned}
 \tilde{Q}_r^- &= \frac{1}{\sqrt{8}} [d_{r+\hat{x}+\hat{y}} - id_{r+\hat{x}} + id_{r+\hat{y}} - d_r \\
 &\quad - ic_{r+\hat{x}+\hat{y}} + c_{r+\hat{x}} - c_{r+\hat{y}} + ic_r], \\
 P_r^+ &= \frac{1}{\sqrt{8}} [-d_{r+\hat{x}+\hat{y}} - id_{r+\hat{x}} + id_{r+\hat{y}} + d_r \\
 &\quad - ic_{r+\hat{x}+\hat{y}} - c_{r+\hat{x}} + c_{r+\hat{y}} + ic_r], \\
 P_r^- &= \frac{1}{\sqrt{8}} [-d_{r+\hat{x}+\hat{y}} - id_{r+\hat{x}} - id_{r+\hat{y}} - d_r \\
 &\quad - ic_{r+\hat{x}+\hat{y}} - c_{r+\hat{x}} - c_{r+\hat{y}} - ic_r], \\
 \tilde{P}_r^+ &= \frac{1}{\sqrt{8}} [d_{r+\hat{x}+\hat{y}} + id_{r+\hat{x}} - id_{r+\hat{y}} - d_r \\
 &\quad - ic_{r+\hat{x}+\hat{y}} - c_{r+\hat{x}} + c_{r+\hat{y}} + ic_r], \\
 \tilde{P}_r^- &= \frac{1}{\sqrt{8}} [d_{r+\hat{x}+\hat{y}} + id_{r+\hat{x}} + id_{r+\hat{y}} + d_r \\
 &\quad - ic_{r+\hat{x}+\hat{y}} - c_{r+\hat{x}} - c_{r+\hat{y}} - ic_r]. \quad (2)
 \end{aligned}$$

By the straightforward calculation, it is verified that all eight operators in Eqs. (2) and their Hermitian conjugates located at the same cube anticommute with each other except for the commutators such as $\{Q_r^{+\dagger}, Q_r^+\} = 1$, etc. However, some of them located at adjacent cubes do not commute with each other, such as $\{Q_r^{+\dagger}, Q_{r+\hat{x}+\hat{y}}^-\} = 1/4$, etc. This comes from the fact that the number of sites doubles that of the cubes. Therefore, a suitable assignment of locations of the cube operators is required to construct the target projective Hamiltonian, which can be carried out by considering symmetry transformations. See later discussion in Sec. III. Here, it should be emphasized that the use of the cubic operators is essential for constructing the bilayer models. In other words, operators defined on plaquettes cannot be introduced for it. Therefore, the bilayer models introduced in the following section cannot be transformed to systems with unconnected unit cells (see, e.g., Fig. 4).

B. Time-reversal symmetry of eight cube operators

Before going to the model construction, we introduce a time-reversal symmetry (\mathcal{T}) for the second quantized operators [42] as follows, which plays an important role in later discussions:

$$\mathcal{T}i\mathcal{T}^{-1} = -i, \quad \mathcal{T}c_r\mathcal{T}^{-1} = d_r, \quad \mathcal{T}d_r\mathcal{T}^{-1} = c_r. \quad (3)$$

From Eqs. (3), the transformation of cube operators is induced. It is easily verified that $\mathcal{T}Q_r^+\mathcal{T}^{-1} = -iQ_r^+$, etc. The above time-reversal symmetry in Eqs. (3) is reminiscent of that of the quantum spin Hall effect. In fact, fermions c_r and d_r correspond to spin-up and spin-down electrons, respectively, and $\mathcal{T}^2 = -1$ in both systems.

LIOMs are given as the number operators of the above ℓ -bits, Q_r^+ through \tilde{P}_r^- :

$$\begin{aligned}
 K_r^+ &= Q_r^{+\dagger} Q_r^+, & K_r^- &= Q_r^{-\dagger} Q_r^-, \\
 \tilde{K}_r^+ &= \tilde{Q}_r^{+\dagger} \tilde{Q}_r^+, & \tilde{K}_r^- &= \tilde{Q}_r^{-\dagger} \tilde{Q}_r^-, \quad (4)
 \end{aligned}$$

$$\begin{aligned}
 M_r^+ &= P_r^{+\dagger} P_r^+, & M_r^- &= P_r^{-\dagger} P_r^-, \\
 \tilde{M}_r^+ &= \tilde{P}_r^{+\dagger} \tilde{P}_r^+, & \tilde{M}_r^- &= \tilde{P}_r^{-\dagger} \tilde{P}_r^-. \quad (5)
 \end{aligned}$$

All the LIOMs in Eqs. (4) and (5) are invariant under the time-reversal transformation \mathcal{T} in Eqs. (3). The Hamiltonians are to be constructed via the above LIOMs. We require the

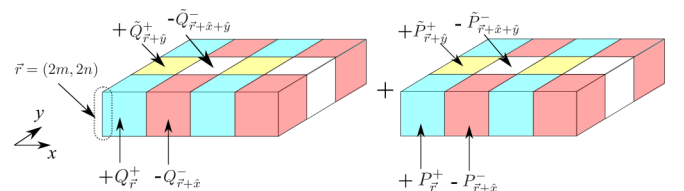


FIG. 3. Schematic picture of the Hamiltonian of the bilayer system given by Eq. (12). The unit cell is 2×2 , which contains four cubes.

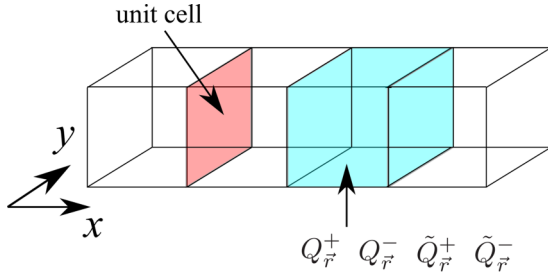


FIG. 4. Schematic picture of the Hamiltonian of a square prism given by Eq. (16). Each cube contains four cube operators, $Q_{\vec{r}}^+$ through $\tilde{Q}_{\vec{r}}^-$.

target systems to have topological properties. In other words, on the construction of the Hamiltonian, we require to assign the system to some topological class in a tenfold way [43]. To this end, we impose chiral symmetry on the Hamiltonians, which is discussed in the following section.

C. Chiral symmetries of eight cube operators

The next step is to assign locations of these cubes to define the Hamiltonian with nontrivial topology. It is possible to construct various models for it by means of the eight cube operators. In the following, we show some of them. We impose chiral symmetry \mathcal{S} to the target models. With a transformation using a unitary operator \mathcal{U} , chiral symmetry requires that the (second quantized) Hamiltonian H transforms as [42]

$$(\mathcal{U}K)H(\mathcal{U}K)^{-1} = \mathcal{U}H^*\mathcal{U}^{-1} = H, \quad (6)$$

where K is the complex conjugation and \mathcal{O}^* denotes the complex conjugate of the operator \mathcal{O} . The chiral operator is given by $\mathcal{S} = \mathcal{U}K$, which is an *antiunitary operator* [42]. The operator \mathcal{S} plays an important role in the construction of topological models.

Here, as a candidate of the unitary operator \mathcal{U} in \mathcal{S} , we can introduce two unitary operators \mathcal{S}_x and \mathcal{S}_y . Under \mathcal{S}_x for $\vec{r} = (x = \text{even}, y)$,

$$\begin{aligned} c_{\vec{r}} &\rightarrow ic_{\vec{r}+\hat{x}}^\dagger, & c_{\vec{r}+\hat{x}} &\rightarrow -ic_{\vec{r}+2\hat{x}}^\dagger, \\ c_{\vec{r}+\hat{y}} &\rightarrow ic_{\vec{r}+\hat{x}+\hat{y}}^\dagger, & c_{\vec{r}+\hat{x}+\hat{y}} &\rightarrow -ic_{\vec{r}+2\hat{x}+\hat{y}}^\dagger, \\ d_{\vec{r}} &\rightarrow id_{\vec{r}+\hat{x}}^\dagger, & d_{\vec{r}+\hat{x}} &\rightarrow -id_{\vec{r}+2\hat{x}}^\dagger, \\ d_{\vec{r}+\hat{y}} &\rightarrow id_{\vec{r}+\hat{x}+\hat{y}}^\dagger, & d_{\vec{r}+\hat{x}+\hat{y}} &\rightarrow -id_{\vec{r}+2\hat{x}+\hat{y}}^\dagger. \end{aligned} \quad (7)$$

In order to construct symmetric Hamiltonians under $\mathcal{S}_x K$, the following properties are useful:

$$\begin{aligned} \mathcal{S}_x(Q_{\vec{r}}^+)^*\mathcal{S}_x^{-1} &= -i(Q_{\vec{r}+\hat{x}}^-)^\dagger, \\ \mathcal{S}_x(Q_{\vec{r}}^-)^*\mathcal{S}_x^{-1} &= -i(Q_{\vec{r}+\hat{x}}^+)^\dagger, \\ \mathcal{S}_x(\tilde{Q}_{\vec{r}}^+)^*\mathcal{S}_x^{-1} &= -i(\tilde{Q}_{\vec{r}+\hat{x}}^-)^\dagger, \\ \mathcal{S}_x(\tilde{Q}_{\vec{r}}^-)^*\mathcal{S}_x^{-1} &= -i(\tilde{Q}_{\vec{r}+\hat{x}}^+)^\dagger, \end{aligned} \quad (8)$$

and similarly for $\{P_{\vec{r}}\}$'s. In the ordinary chiral symmetry, the unitary matrix \mathcal{U} operates on internal symmetries. In the present case, however, \mathcal{S}_x operates on the site index and therefore it is a kind of generalized translation operator in the x direction. As a result, some specific choice of the coefficients

is required in the transformation in Eqs. (7) coming from the built-up definition of the cube operators Q and P defined in Eqs. (2).

Transformation \mathcal{S}_y can be defined similarly for $\vec{r} = (x, y = \text{even})$,

$$\begin{aligned} c_{\vec{r}} &\rightarrow -ic_{\vec{r}+\hat{y}}^\dagger, & c_{\vec{r}+\hat{x}} &\rightarrow -ic_{\vec{r}+\hat{x}+\hat{y}}^\dagger, \\ c_{\vec{r}+\hat{y}} &\rightarrow -ic_{\vec{r}+2\hat{y}}^\dagger, & c_{\vec{r}+\hat{x}+\hat{y}} &\rightarrow -ic_{\vec{r}+\hat{x}+2\hat{y}}^\dagger, \\ d_{\vec{r}} &\rightarrow id_{\vec{r}+\hat{y}}^\dagger, & d_{\vec{r}+\hat{x}} &\rightarrow id_{\vec{r}+\hat{x}+\hat{y}}^\dagger, \\ d_{\vec{r}+\hat{y}} &\rightarrow id_{\vec{r}+2\hat{y}}^\dagger, & d_{\vec{r}+\hat{x}+\hat{y}} &\rightarrow id_{\vec{r}+\hat{x}+2\hat{y}}^\dagger, \end{aligned} \quad (9)$$

and under \mathcal{S}_y ,

$$\begin{aligned} \mathcal{S}_y(Q_{\vec{r}}^+)^*\mathcal{S}_y^{-1} &= -i(\tilde{Q}_{\vec{r}+\hat{y}}^+)^\dagger, \\ \mathcal{S}_y(Q_{\vec{r}}^-)^*\mathcal{S}_y^{-1} &= -i(\tilde{Q}_{\vec{r}+\hat{y}}^-)^\dagger, \\ \mathcal{S}_y(\tilde{Q}_{\vec{r}}^+)^*\mathcal{S}_y^{-1} &= -i(Q_{\vec{r}+\hat{y}}^+)^\dagger, \\ \mathcal{S}_y(\tilde{Q}_{\vec{r}}^-)^*\mathcal{S}_y^{-1} &= -i(Q_{\vec{r}+\hat{y}}^-)^\dagger, \end{aligned} \quad (10)$$

and similarly for $\{P_{\vec{r}}\}$'s. The \mathcal{S}_y again induces a translation in the y direction. This is the origin of the slight difference between \mathcal{S}_x and \mathcal{S}_y .

As we show in the following sections, we employ \mathcal{S}_x as a guiding principle for constructing model Hamiltonians. (Chiral symmetry \mathcal{S}_y is less effective for the construction. Imposing both of them is incompatible for bilayer models. See later discussion.)

III. MODELS AND THEIR HAMILTONIAN

A. Models on two-dimensional bilayer lattice

By using transformation properties of $\{Q\}$'s and $\{P\}$'s obtained in the previous section [Eqs. (8)], we can construct various models. As we are interested in the fully localized system with a topological phase, the symmetry \mathcal{S}_x or \mathcal{S}_y can be a guiding principle for constructing the Hamiltonian, which is composed of the LIOMs, i.e., $K_{\vec{r}}^\pm$, etc., in Eqs. (4) and (5). In order to construct models, the following facts have to be taken into account:

(A) Under the transformation in Eqs. (7), the LIOMs transform such as

$$\begin{aligned} K_{\vec{r}}^+ &\rightarrow Q_{\vec{r}+\hat{x}}^-(Q_{\vec{r}+\hat{x}}^-)^\dagger = -(Q_{\vec{r}+\hat{x}}^-)^\dagger Q_{\vec{r}+\hat{x}}^- + 1, \\ &= -K_{\vec{r}+\hat{x}}^- + 1, \text{ etc.} \end{aligned} \quad (11)$$

(B) For commutativity of the LIOMs, $\{K_{\vec{r}}\}$ and $\{P_{\vec{r}}\}$ at the same location does not guarantee that they all commute with each other. For example, $K_{\vec{r}}^+$ does not commute with $K_{\vec{r}+\hat{x}+\hat{y}}^-$.

From condition A, signs of the LIOMs in the Hamiltonian have to be determined suitably to cancel the additional constant in Eq. (11). From condition B, $\{K_{\vec{r}}\}$ and $\{P_{\vec{r}}\}$ should be call *quasi-LIOMs*, although the Hamiltonian is to be constructed to commute with all of them. There exists a certain ‘‘selection rule’’ such that $(Q_{\vec{r}}^+)^\dagger(Q_{\vec{r}+\hat{x}+\hat{y}}^-)|0\rangle$ cannot be an eigenstate of the Hamiltonian. Therefore, suitable assignment of spatial location of the LIOMs is required.

There are still various models that satisfy the above requirements coming from A and B. One of the generic ones

defined on the full bilayer lattice is the following system with Hamiltonian such as

$$H_{\text{BL}} = \sum_{m,n} \sum_{\vec{r}=(2m,2n)} \left(\tau_K [K_{\vec{r}}^+ - K_{\vec{r}+\hat{x}}^- + \tilde{K}_{\vec{r}+\hat{y}}^+ - \tilde{K}_{\vec{r}+\hat{x}+\hat{y}}^-] + \tau_M [M_{\vec{r}}^+ - M_{\vec{r}+\hat{x}}^- + \tilde{M}_{\vec{r}+\hat{y}}^+ - \tilde{M}_{\vec{r}+\hat{x}+\hat{y}}^-] \right), \quad (12)$$

where τ_K and τ_M are arbitrary real parameters, and (n, m) are integers. The spatial structure of H_{BL} is schematically shown in Fig. 3. The parameters τ_K and τ_M can be site dependent as long as they satisfy the symmetry $\mathcal{S}_x K$, such as $(\tau_K, \tau_M) \rightarrow (\tau_{K,n}, \tau_{M,n})$, but we consider the uniform case in this work. Expression of H_{BL} in terms of the original fermions, $c_{\vec{r}}$ and $d_{\vec{r}}$, is obtained by substituting Eqs. (2), (4), and (5) into H_{BL} in Eq. (12). With the periodic boundary condition, the number of the LIOMs in H_{BL} is extensive, and all energy eigenstates are localized and given as $(Q_{2m,2n}^+)^{\dagger}|0\rangle$, etc.

Here, let us consider the symmetries of the Hamiltonian H_{BL} . Since the model construction is carried out with respect to the chiral symmetry $\mathcal{S}_x K$, the second quantized Hamiltonian H_{BL} is chiral symmetric. Also, we easily notice that the Hamiltonian H_{BL} has the time-reversal symmetry \mathcal{T} , defined in the previous section. Furthermore, in the usual sense in the topological classification [42], the chiral transformation $\mathcal{S}_x K$ is to be given by the product of the time-reversal transformation \mathcal{T} and a particle-hole transformation \mathcal{C} . Hence, we also can directly notice the presence of the particle-hole transformation \mathcal{C} given as $\mathcal{T}^{-1} \mathcal{S}_x K$. Therefore, the Hamiltonian H_{BL} has \mathcal{T} , \mathcal{C} , and $\mathcal{S}_x K$ symmetries. This fact implies that the Hamiltonian H_{BL} belongs to the BDI class in the tenfold way [43]. As far as the topological classification [41], this fact indicates that the model H_{BL} can exhibit a topological phase and some gapless edge states for a certain lattice geometry. In later sections, we discuss such topological aspects, some of which are substantially related to the full-localization properties.

Furthermore for the system of H_{BL} , nontrivial interactions can be introduced, which preserve the localization properties and chiral symmetry $\mathcal{S}_x K$. One of them is given by

$$H_{\text{BLI}} = g \sum_{m,n} \sum_{\vec{r}=(2m,2n)} [K_{\vec{r}}^+ K_{\vec{r}+\hat{x}}^- + \tilde{K}_{\vec{r}+\hat{y}}^+ \tilde{K}_{\vec{r}+\hat{x}+\hat{y}}^- - K_{\vec{r}}^+ \tilde{K}_{\vec{r}+\hat{y}}^+ - K_{\vec{r}+\hat{x}}^- \tilde{K}_{\vec{r}+\hat{x}+\hat{y}}^- + (K \rightarrow M)], \quad (13)$$

where g is the coupling constant. The interactions given by H_{BLI} mostly describe scattering processes of $c_{\vec{r}}$ and $d_{\vec{r}}$. Another type of interaction can be introduced by the terms

$$H_{\text{BLII}} = g' \sum_{m,n} \sum_{\vec{r}=(2m,2n)} \left[\left(K_{\vec{r}}^+ - \frac{1}{2} \right) \left(K_{\vec{r}+\hat{x}}^- - \frac{1}{2} \right) + \left(\tilde{K}_{\vec{r}+\hat{y}}^+ - \frac{1}{2} \right) \left(\tilde{K}_{\vec{r}+\hat{x}+\hat{y}}^- - \frac{1}{2} \right) + \left(K_{\vec{r}}^+ - \frac{1}{2} \right) \left(\tilde{K}_{\vec{r}+\hat{y}}^+ - \frac{1}{2} \right) + \left(K_{\vec{r}+\hat{x}}^- - \frac{1}{2} \right) \left(\tilde{K}_{\vec{r}+\hat{x}+\hat{y}}^- - \frac{1}{2} \right) + (K \rightarrow M) \right], \quad (14)$$

which is again invariant under $\mathcal{S}_x K$.

If one discards chiral symmetries but preserves the integrability of models, the interactions with the following form are possible, i.e.,

$$H_{\text{III}} = g'' \sum_{m,n} \sum_{\vec{r}=(2m,2n)} K_{\vec{r}}^+ P_{\vec{r}}^{+\dagger} P_{\vec{r}+\hat{x}}^- + \dots, \quad (15)$$

which are composed of K 's and P 's. In this case, K 's are conserved quantities and can be fixed to certain finite values. In the specific sector, the model reduces to a free system without genuine interaction terms.

B. Models on square prism lattice and topological properties

We have shown that the model of H_{BL} belongs to the BDI class. Hence, if one reduces the model to a certain one-dimensional system without changing the symmetry class, the resultant (quasi-)one-dimensional model has a possibility to exhibit a topological phase characterized by some bulk topological invariant, e.g., winding number, Berry or Zak phase [52], etc. From this point of view, we construct another interesting and also instructive model defined on a square prism lattice, whose Hamiltonian is given as follows (see Fig. 4):

$$H_{\text{SP}} = \sum_{\vec{r}=(n,0)} [\tau_0 [K_{\vec{r}}^+ - K_{\vec{r}}^-] + \tau_1 [\tilde{K}_{\vec{r}}^+ - \tilde{K}_{\vec{r}}^-]], \quad (16)$$

where τ_0 and τ_1 are arbitrary real parameters. The model H_{SP} is invariant under the transformation in Eqs. (7) for $\{c_{\vec{r}}\}$'s with the identification $c_{\vec{r}+2\hat{y}} = c_{\vec{r}}$. The above four LIOMs per unit cube are extensive, and localized single-particle eigenstates are $(Q_{\vec{r}}^+)^{\dagger}|0\rangle, \dots, (\tilde{Q}_{\vec{r}}^-)^{\dagger}|0\rangle$. Nontrivial interactions can be introduced as in the previous work for the Creutz ladder [34].

In later discussion, we study the model in Eq. (16) by numerical methods. To this end, we express the Hamiltonian, H_{SP} , in terms of the original fermions. After some calculation, we obtain

$$H_{\text{SP}} = H_{\text{CL}} + H_{\text{IS1}} + H_{\text{IS2}}, \quad (17)$$

$$H_{\text{CL}} = \sum_{\vec{r}=(n,0)} [i\bar{\tau} (c_{\vec{r}+\hat{x}+\hat{y}}^{\dagger} c_{\vec{r}+\hat{y}} - c_{\vec{r}+\hat{x}}^{\dagger} c_{\vec{r}}) + \bar{\tau} (c_{\vec{r}}^{\dagger} c_{\vec{r}+\hat{x}+\hat{y}} + c_{\vec{r}+\hat{y}}^{\dagger} c_{\vec{r}+\hat{x}}) - i\bar{\tau} (d_{\vec{r}+\hat{x}+\hat{y}}^{\dagger} d_{\vec{r}+\hat{y}} - d_{\vec{r}+\hat{x}}^{\dagger} d_{\vec{r}}) + \bar{\tau} (d_{\vec{r}}^{\dagger} d_{\vec{r}+\hat{x}+\hat{y}} + d_{\vec{r}+\hat{y}}^{\dagger} d_{\vec{r}+\hat{x}})] + \text{H.c.}, \quad (18)$$

$$H_{\text{IS1}} = \sum_{\vec{r}=(n,0)} \Delta (c_{\vec{r}}^{\dagger} d_{\vec{r}+\hat{x}} + c_{\vec{r}+\hat{x}}^{\dagger} d_{\vec{r}} + c_{\vec{r}+\hat{y}}^{\dagger} d_{\vec{r}+\hat{x}+\hat{y}} + c_{\vec{r}+\hat{x}+\hat{y}}^{\dagger} d_{\vec{r}+\hat{y}}) + \text{H.c.}, \quad (19)$$

$$H_{\text{IS2}} = \sum_{\vec{r}=(n,0)} i\Delta (d_{\vec{r}+\hat{x}}^{\dagger} c_{\vec{r}+\hat{y}} + c_{\vec{r}+\hat{x}+\hat{y}}^{\dagger} d_{\vec{r}} + d_{\vec{r}+\hat{y}}^{\dagger} c_{\vec{r}+\hat{x}} + c_{\vec{r}}^{\dagger} d_{\vec{r}+\hat{x}+\hat{y}}) + \text{H.c.}, \quad (20)$$

where $\bar{\tau} = \frac{1}{4}(\tau_0 + \tau_1)$ and $\Delta = \frac{1}{4}(\tau_1 - \tau_0)$. H_{CL} is nothing but the Creutz ladder Hamiltonian of $c_{\vec{r}}$ and $d_{\vec{r}}$, and H_{IS1} and H_{IS2} mix them and vanish for $\tau_0 = \tau_1$.

Let us investigate the topological properties of the noninteracting system of H_{SP} . It is useful to express the Hamiltonian

Eq. (17) in terms of operators in the momentum space for the x direction:

$$\Phi(k_x) \equiv \begin{pmatrix} \tilde{c}(k_x, y=0) \\ \tilde{c}(k_x, y=1) \\ \tilde{d}(k_x, y=0) \\ \tilde{d}(k_x, y=1) \end{pmatrix},$$

where $\tilde{c}(k_x)$'s are Fourier-transformed operators and $H_{\text{SP}} = \int dk_x \Phi^\dagger(k_x) h_{\text{SP}}(k_x) \Phi(k_x)$. Explicitly, $h_{\text{SP}}(k_x)$ is given as

$$h_{\text{SP}}(k_x) = \begin{pmatrix} 2\bar{\tau}s(k) & 2\bar{\tau}c(k) & 2\Delta c(k) & 2\Delta s(k) \\ 2\bar{\tau}c(k) & -2\bar{\tau}s(k) & -2\Delta s(k) & 2\Delta c(k) \\ 2\Delta c(k) & -2\Delta s(k) & -2\bar{\tau}s(k) & 2\bar{\tau}c(k) \\ 2\Delta s(k) & 2\Delta c(k) & 2\bar{\tau}c(k) & 2\bar{\tau}s(k) \end{pmatrix}, \quad (21)$$

where $s(k) \equiv \sin(k_x)$ and $c(k) \equiv \cos(k_x)$.

From Eq. (21), the symmetries of $h_{\text{SP}}(k_x)$ are clear [besides \mathcal{S}_x in Eq. (7)]. First, $h_{\text{SP}}(k_x)$ has the time-reversal symmetry mentioned in Sec. II B,

$$T_b h_{\text{SP}}(k_x) T_b^{-1} = h_{\text{SP}}(-k_x),$$

$$T_b = K \begin{pmatrix} 0 & \mathbf{1}_2 \\ \mathbf{1}_2 & 0 \end{pmatrix}, \quad (22)$$

where K is a complex conjugate operator and $\mathbf{1}_2$ is a 2×2 identity matrix. Hence, T_b is antiunitary.

Second, $h_{\text{SP}}(k_x)$ has a particle-hole symmetry,

$$C_b h_{\text{SP}}(k_x) C_b^{-1} = -h_{\text{SP}}(-k_x),$$

$$C_b = \begin{pmatrix} 0 & -i\sigma_y \\ i\sigma_y & 0 \end{pmatrix}, \quad (23)$$

where σ_y is the y component of the Pauli matrix. Hence, C_b is unitary.

Third, $h_{\text{SP}}(k_x)$ has a chiral symmetry given by the chiral operator $S_b = T_b C_b$,

$$S_b h_{\text{SP}}(k_x) S_b^{-1} = -h_{\text{SP}}(k_x),$$

$$S_b = K \begin{pmatrix} \sigma_y & 0 \\ 0 & -\sigma_y \end{pmatrix}, \quad (24)$$

where S_b is antiunitary. From these symmetries, $h_{\text{SP}}(k_x)$ belongs to the BDI class in the tenfold way [41,43].

Furthermore, the system H_{SP} also has a spatial reflection (inversion) symmetry, which is given by

$$I h_{\text{SP}}(k_x) I^{-1} = h_{\text{SP}}(-k_x),$$

$$I = \begin{pmatrix} \sigma_x & 0 \\ 0 & \sigma_x \end{pmatrix}, \quad (25)$$

where σ_x is the x -component of the Pauli matrix. This reflection symmetry plays an important role for the quantization of the Berry (Zak) phase [53,54], which acts as a topological index in this system.

We numerically demonstrate the topological properties of $h_{\text{SP}}(k_x)$. By diagonalizing $h_{\text{SP}}(k_x)$, we can obtain energy eigenvalues as shown in Fig. 5(a). Certainly, there appear four flat bands. Here, we calculate the Berry phase [52] given by $\gamma_M = i \int_{-\pi}^{\pi} \langle u_\ell(k_x) | \partial_{k_x} | u_\ell(k_x) \rangle dk_x$, where $|u_\ell(k_x)\rangle$ is the ℓ th eigenstate of $h_{\text{SP}}(k_x)$. For each flat band, γ_M takes π ; that is, each band is nontrivial. This quantization comes from the

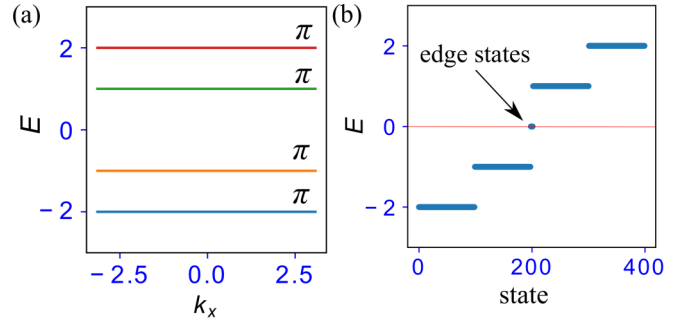


FIG. 5. (a) Energy eigenvalues of H_{SP} for $\tau_0 = 2$ and $\tau_1 = 1$ for the periodic boundary condition. There exist four flat bands. The numbers near each band show γ_M , the Berry phase. All flat bands are topologically nontrivial. (b) Energy eigenvalues under the open boundary condition. Fourfold zero-energy edge states appear.

inversion symmetry I (crystalline topological insulator [55]). We show another Berry phase obtained by introducing boundary twist in a later section.

Here, we also show the energy spectrum by diagonalizing H_{SP} under the OBC in Fig. 5(b). The result indicates the existence of the gapless edge modes, which are discussed in Sec. IV.

We introduce the following ‘‘interleg’’ hopping, which respects the symmetries of the Hamiltonian H_{SP} in Eqs. (7),

$$H_v = v \sum_{\vec{r}=(n,0)} (c_{\vec{r}+\hat{y}}^\dagger c_{\vec{r}} + d_{\vec{r}+\hat{y}}^\dagger d_{\vec{r}} + \text{H.c.}), \quad (26)$$

where v is an arbitrary real parameter. It should be noted that Eq. (26) does not break the chiral and reflection symmetries. In the previous works on the Creutz ladder, we showed that the hopping H_v makes all states extended even for infinitesimal v . However, needless to say, the symmetries for topological properties are preserved, thus bulk-band topology does not change without gap closing. Also, we expect that the corresponding gapless edge modes are preserved even for finite v .

It is interesting and also important to examine if there exist interactions that respect the \mathcal{S}_x symmetry [Eqs. (7)]. To search for them, Eq. (11) is quite useful. There are several forms of the interactions, and we display a typical one:

$$H_{\text{SPI}} = \lambda \sum_{\vec{r}} \left[\left(K_{\vec{r}}^+ - \frac{1}{2} \right) \left(K_{\vec{r}+\hat{x}}^+ - \frac{1}{2} \right) + \left(K_{\vec{r}}^- - \frac{1}{2} \right) \left(K_{\vec{r}+\hat{x}}^- - \frac{1}{2} \right) + \left(\tilde{K}_{\vec{r}}^+ - \frac{1}{2} \right) \left(\tilde{K}_{\vec{r}+\hat{x}}^+ - \frac{1}{2} \right) + \left(\tilde{K}_{\vec{r}}^- - \frac{1}{2} \right) \left(\tilde{K}_{\vec{r}+\hat{x}}^- - \frac{1}{2} \right) \right], \quad (27)$$

where λ is a coupling constant. Here, it should be noted that the above interaction H_{SPI} [Eq. (27)] is invariant under transformations in Eqs. (22)–(25) as well as $\mathcal{S}_x K$. Therefore, we expect that the interaction H_{SPI} plays an important role for the emergence of gapless edge modes as verified later on. There, we also explain that a phase transition takes place as the

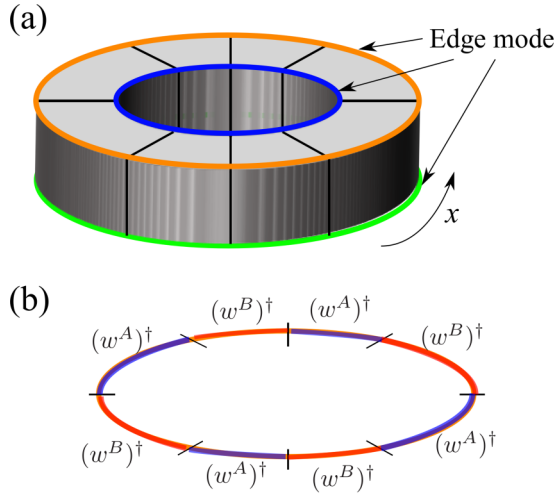


FIG. 6. (a) Coarse-grained schematic picture of the bilayer system with open boundary condition of thin cylinder (disk) shape. (b) There emerge four edge modes, each of which is one dimensional and a linear combination of $(w^A)^\dagger$'s or $(w^B)^\dagger$'s.

parameter λ is varied. Discussion on topological properties of the system will be given as well.

In later numerical study on the Hamiltonian H_{SP} , we study effects of the following interactions, which are invariant under the transformations in Eqs. (22)–(25):

$$H_{II} = V \sum_{\vec{r}} [n_{\vec{r}}^c n_{\vec{r}+\hat{y}}^c + n_{\vec{r}}^c n_{\vec{r}+\hat{x}}^c + n_{\vec{r}+\hat{y}}^c n_{\vec{r}+\hat{x}+\hat{y}}^c + (c \rightarrow d)], \quad (28)$$

where V is an arbitrary real parameter, and $n_{\vec{r}}^c = c_{\vec{r}}^\dagger c_{\vec{r}}$, $n_{\vec{r}}^d = d_{\vec{r}}^\dagger d_{\vec{r}}$. The interactions H_{II} in Eq. (28) seem to break the \mathcal{S}_x symmetry in Eqs. (7). In fact, under Eqs. (7) there appear terms such as $\sum_{\vec{r}} [n_{\vec{r}}^c + n_{\vec{r}+\hat{x}}^c + n_{\vec{r}+\hat{y}}^c + n_{\vec{r}+\hat{x}+\hat{y}}^c + (c \rightarrow d)]$, in addition to a constant. However, as we always consider the system with fixed particle number, these terms are irrelevant. Furthermore, the additional constant in the Hamiltonian does not change wave functions of energy eigenstates, so it is also irrelevant. Therefore, we expect the stability of topological properties of the Hamiltonian H_{SP} in the presence of H_{II} , as long as it does not change the band structure. This expectation will be verified by the numerical calculation later on.

IV. EDGE MODES

In the previous section, we have introduced models H_{BL} and H_{SP} of full localization in the bulk and belonging to the BDI class. Then, it is expected that there appear gapless edge modes in the above models in the OBC. Depending on the geometrical structure of the systems, gapless edge modes emerge in a different way. Then, we discuss the models H_{BL} and H_{SP} , separately.

Let us first consider the model H_{BL} in a thin cylinder lattice whose schematic picture is displayed in Fig. 6. In the x direction, the system is periodic, whereas in the y direction, the boundaries exist. One may expect that gapless edge modes appear in the boundary surfaces, but this is not the case. They exist in the four edges of the cylinder [see Fig. 6(a)].

From Fig. 3, these edges of the cylinder are composed of edges of a sequence of $\{K\}$'s such as $(\cdots K^+ K^- K^+ K^- \cdots)$ or $(\cdots \tilde{K}^+ \tilde{K}^- \tilde{K}^+ \tilde{K}^- \cdots)$ (and also sequences of $\{M\}$'s). Then from Fig. 2, the terms in the Hamiltonian corresponding to the boundaries of the upper plane are given by

$$h_B = \tau_{K(M)} \sum_{\vec{r} \in \mathcal{C}} [(\omega_{\vec{r},\hat{x}}^{A\dagger} \omega_{\vec{r},\hat{x}}^A) - (\omega_{\vec{r}+\hat{x},\hat{x}}^{B\dagger} \omega_{\vec{r}+\hat{x},\hat{x}}^B)] + \cdots,$$

where \mathcal{C} represents one of the two closed edges in the upper plane, and \sum' denotes the restricted summation such as $\vec{r} = (x = \text{even}, y = \text{location of edge})$. (A similar boundary Hamiltonian of the lower edge is obtained by the time-reversal transformation, and then $\omega^{A/B} \rightarrow \tilde{\omega}^{A/B}$.) The boundary Hamiltonian h_B does not contain $\omega_{\vec{r},\hat{x}}^B$ and $\omega_{\vec{r}+\hat{x},\hat{x}}^A$. Therefore, the zero modes are created by the operators satisfying the following equation [see Fig. 6(b)]:

$$\mathcal{B}_C = \sum_{\vec{r} \in \mathcal{C}} \alpha_{\vec{r}} \omega_{\vec{r},\hat{x}}^{B\dagger} = \sum_{\vec{r} \in \mathcal{C}} \alpha_{\vec{r}+\hat{x}} \omega_{\vec{r}+\hat{x},\hat{x}}^{A\dagger}, \quad (29)$$

where $\{\alpha_{\vec{r}}\}$'s are suitably chosen phase factors as \mathcal{B}_C commutes with the boundary Hamiltonian h_B . (The commutativity between \mathcal{B}_C and the other parts of the Hamiltonian H_{SP} is obvious.) It should be remarked that this commutativity is preserved even in the presence of the interactions H_{BLI} and H_{BLII} in Eqs. (13) and (14). The above operator on \mathcal{C} , \mathcal{B}_C , is a linear combination of $c_{\vec{r}}^\dagger$ with suitably chosen coefficients. For example for a square edge with four sites $(1, \dots, 4)$, we have $\mathcal{B}_C^\dagger = c_1^\dagger + ic_2^\dagger + c_3^\dagger + ic_4^\dagger = (c_1^\dagger + ic_2^\dagger) + (c_3^\dagger + ic_4^\dagger) = i(c_2^\dagger - ic_3^\dagger) + i(c_4^\dagger - ic_1^\dagger)$ [see Eq. (29)]. It is obvious that in general, \mathcal{B}_C can be constructed consistently with the condition in Eq. (29) because \mathcal{C} is composed of an even number of sites. It is also verified that \mathcal{B}_C transforms suitably under chiral symmetry transformation [$\mathcal{S}_x K$ in Eqs. (7)]:

$$\begin{aligned} \mathcal{S}_x (\mathcal{B}_C^\dagger)_C \mathcal{S}_x^{-1} &= \mathcal{S}_x (c_1^\dagger - ic_2^\dagger + c_3^\dagger - ic_4^\dagger) \mathcal{S}_x^{-1} \\ &= -ic_2 + c_3 - ic_4 + c_1 \\ &= (c_1^\dagger + ic_2^\dagger + c_3^\dagger + ic_4^\dagger)^\dagger \\ &= \mathcal{B}_C. \end{aligned} \quad (30)$$

The origin of this *one-dimensional gapless edge mode* is closely related to flat-band localization, and will be discussed in detail in Sec. VI, after examining the model of H_{SP} . Here, we should note that seen from the form of Eq. (29) the above edge zero modes survive under the additional open boundary condition in the x direction even though the $\mathcal{S}_x K$ symmetry is explicitly broken at the edges of the x direction.

A few comments are in order. There are four boundary modes, \mathcal{B}_C^a ($a = 1, 2, 3, 4$), where the suffix a denotes the four edges of the cylinder. In the previous works [48], it was argued that gapless edge modes are stable *even at finite temperature* if all the other bulk states are localized. The present bilayer model has such properties even though the gapless edge modes are a linear combination of the original particles.

As discussed in Ref. [56] for one-dimensional models, SYK-type models can be constructed via \mathcal{B}_C 's. There, fourth-order terms of them are leading because of chiral symmetry given in Eq. (30). In the original work of the SYK model, this symmetry was imposed by hand, but it emerges naturally

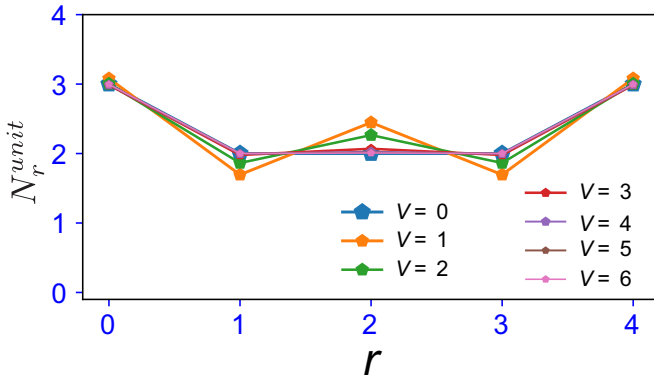


FIG. 7. Density profile of half-filled state + two particles for various interaction strength V . We plot the total density of the unit cell, $N_r^{unit} = n_{r+y}^c + n_r^c + n_{r+y}^d + n_r^d$. Edge modes are quite stable against the repulsion. The system size is $L = 5$ (20 sites) with 12 particles.

in the present system. A possible effective Hamiltonian is such that $H = \sum V_{abcd} \mathcal{B}^{a\dagger} \mathcal{B}^{b\dagger} \mathcal{B}^c \mathcal{B}^d$, where the edge index $(a-d) = (1-4)$ and the coefficients V_{abcd} are complex random numbers. The classification of the above model for *ordinary complex particles* has been already done in Ref. [56].

Next, let us consider the model H_{SP} in Eq. (16) with the OBC such as $0 \leq x \leq L-1$. There are four edge modes, which are given by $(\omega_{x=0,y}^A)^{\dagger}|0\rangle$, $(\tilde{\omega}_{x=0,y}^B)^{\dagger}|0\rangle$, $(\omega_{x=L,y}^B)^{\dagger}|0\rangle$, and $(\tilde{\omega}_{x=L,y}^A)^{\dagger}|0\rangle$ [see Fig. 5(b)]. Even in the presence of the interactions H_{SP1} in Eq. (27), the four operators $(\omega_{x=0,y}^A, \dots, \tilde{\omega}_{x=L,y}^A)$ commute exactly with the Hamiltonian $H_{SP} + H_{SP1}$. This indicates that the gapless edge modes survive in the interacting system.

We also study effects of the interactions H_{II} [Eq. (28)] by numerical methods [57]. In particular as the above edge-mode creation operators do not commute with H_{II} , we are interested in stability of the edge modes. In Fig. 7, we display the density profiles for various values of V for the half-filled state + two particles. The additional two particles on top of the half-filled state are expected to correspond to the gapless edge modes. Numerical calculations obviously show the stability of the edge modes even for large V . We think that this result comes from the fact that H_{II} preserves symmetries, as we discussed in the above, and then it enhances homogeneity of the bulk regime.

In the following section, we investigate topological indices corresponding to the model $H_{SP} + H_{SP1}$ in Eqs. (16) and (27).

V. BULK TOPOLOGICAL INDICES AND STRING OPERATOR

In the previous section, we found that the gapless edge modes emerge under the OBC in the model H_{SP} . This fact implies that the present systems include SPT phases. We further investigate topological indices characterizing topological properties of the model H_{SP} in Eq. (16), i.e., Berry phases obtained from a local twist, string order, etc.

In the momentum representation, we mention that the Berry phase in the H_{SP} system, γ_M , is quantized because of the reflection symmetry in Eqs. (25), and take $\gamma_M = 0, \pi \pmod{2\pi}$. Obtained results of γ_M are shown in Fig. 5.

Here, we employ another method for calculating the Berry phase, which can be used for interacting systems.

To this end, we introduce local twist with $\theta \in (S^1: [0, 2\pi))$ for *all* the hopping terms in H_{SP} residing on certain unit cells. Under this local twist, the Hamiltonian H_{SP} depends on θ , that is, $H_{SP}(\theta)$. For the Hamiltonian $H_{SP}(\theta)$, if the ground state is unique and gapped for all θ , then the Z_2 Berry phase [58–63] from the local twist is given by

$$\gamma_L = i \int_0^{2\pi} d\theta \langle g(\theta) | \partial_\theta | g(\theta) \rangle, \quad (31)$$

where $|g(\theta)\rangle$ is the gapped unique ground state for $H_{SP}(\theta)$. Here, we should note that the Berry phase is defined mod 2π [59]. In the present system, the Berry phase γ_L can be analytically treated since the exact many-body ground state of H_{SP} is already known. The ground state is also useful for the study on the interacting case with H_{SP1} and H_{II} in Eqs. (27) and (28).

To calculate Berry phases practically, we introduce the following twisted hopping in the cube operators at site $\vec{r} = \vec{0} = (0, 0)$:

$$Q_0^+(\theta) = \frac{1}{\sqrt{8}} [-e^{i\theta} d_{\vec{0}+\hat{x}+\hat{y}} + ie^{i\theta} d_{\vec{0}+\hat{x}} + id_{\vec{0}+\hat{y}} - d_0 - ie^{i\theta} c_{\vec{0}+\hat{x}+\hat{y}} + e^{i\theta} c_{\vec{0}+\hat{x}} + c_{\vec{0}+\hat{y}} - ic_0], \quad (32)$$

and similarly for $Q_0^-(\theta)$, $\tilde{Q}_0^+(\theta)$, and $\tilde{Q}_0^-(\theta)$. In fact in the Hamiltonian with the twist $H(\theta)$, the hopping terms in the x direction are changed to $K_0^+(\theta) \equiv (Q_0^+(\theta))^{\dagger} Q_0^+(\theta) \propto e^{-i\theta} d_{\vec{0}+\hat{x}+\hat{y}}^{\dagger} d_{\vec{0}+\hat{y}} + \dots$. It is easy to verify that the above twisted operators satisfy the same commutation relations with the operators for $\theta = 0$, i.e.,

$$\{(Q_0^+(\theta))^{\dagger}, Q_0^+(\theta)\} = 1, \{(Q_0^+(\theta))^{\dagger}, Q_r^{\pm}\} = 0,$$

for $\vec{r} \neq \vec{0}$, etc. Then, operators $K_0^+(\theta)$, etc., which are composed of $Q_0^+(\theta)$, etc., are LIOMs, and energy eigenstates are given by $Q_0^{+\dagger}(\theta)|0\rangle$, etc.

As an example, we first consider the ground state at 1/4 filling for $\tau_0 > \tau_1$, whose wave function is given by

$$|\psi_1(\theta)\rangle = [Q_0^-(\theta)]^{\dagger} \prod_{\vec{r} \neq \vec{0}} Q_{\vec{r}}^{\dagger} |0\rangle. \quad (33)$$

It is easily verified that the energy gap between $|\psi_1(\theta)\rangle$ and the excited states does not close for any $\theta \in [0, 2\pi]$. Then,

$$\begin{aligned} i\gamma_L &= \int_0^{2\pi} d\theta \langle \psi_1(\theta) | \partial_\theta | \psi_1(\theta) \rangle \\ &= i \frac{1}{8} \int_0^{2\pi} d\theta \langle 0 | [-e^{i\theta} d_{\vec{0}+\hat{x}+\hat{y}} + ie^{i\theta} d_{\vec{0}+\hat{x}} - ie^{i\theta} c_{\vec{0}+\hat{x}+\hat{y}} + e^{i\theta} c_{\vec{0}+\hat{x}}]^{\dagger} \\ &\quad \times [-e^{i\theta} d_{\vec{0}+\hat{x}+\hat{y}} + ie^{i\theta} d_{\vec{0}+\hat{x}} - ie^{i\theta} c_{\vec{0}+\hat{x}+\hat{y}} + e^{i\theta} c_{\vec{0}+\hat{x}}] | 0 \rangle \\ &= i\pi. \end{aligned} \quad (34)$$

Therefore, $\gamma_L = \pi$ for the ground state at 1/4 filling. The same result has been obtained by using the momentum representation of the Hamiltonian H_{SP} [see Fig. 5(a)] in Sec. III B. On

the other hand, for the case $\tau_1 > \tau_0$, the ground state is given as

$$|\psi_2(\theta)\rangle = [\tilde{Q}_0^-(\theta)]^\dagger \prod_{\bar{r} \neq \bar{0}} \tilde{Q}_{\bar{r}}^{-\dagger} |0\rangle. \quad (35)$$

Similar calculation to the above shows that the Berry phase of $|\psi_2(\theta)\rangle$ is $\gamma_L = \pi$. Transition between $|\psi_1(\theta)\rangle$ and $|\psi_2(\theta)\rangle$ takes place at $\tau_0 = \tau_1$. At this transition point $\Delta = 0$, the system is simply two independent Creutz ladder fermions, and there appears tremendous degeneracy. As a result, the Berry phase cannot be defined properly.

Let us turn to the half-filling case. The ground-state wave function is given as

$$|\psi_3(\theta)\rangle = [Q_0^-(\theta)]^\dagger [\tilde{Q}_0^-(\theta)]^\dagger \prod_{\bar{r} \neq \bar{0}} Q_{\bar{r}}^{-\dagger} \tilde{Q}_{\bar{r}}^{-\dagger} |0\rangle. \quad (36)$$

The Berry phase is calculated as

$$\begin{aligned} i\gamma_L &= \int_0^{2\pi} d\theta \langle 0 | [Q_0^-(\theta)] [\tilde{Q}_0^-(\theta)] \partial_\theta [[Q_0^-(\theta)]^\dagger [\tilde{Q}_0^-(\theta)]^\dagger] |0\rangle \\ &= \frac{1}{16} \int_0^{2\pi} d\theta \langle 0 | [D(\theta)C(\theta)] \partial_\theta [[C(\theta)]^\dagger [D(\theta)]^\dagger] |0\rangle \\ &= \frac{1}{4} \int_0^{2\pi} d\theta \langle 0 | [C(\theta) \partial_\theta C^\dagger(\theta) + D(\theta) \partial_\theta D^\dagger(\theta)] |0\rangle \\ &= i2\pi \\ &= 0 \pmod{2\pi}, \end{aligned} \quad (37)$$

where $C(\theta) = -ie^{i\theta} c_{\bar{r}+\hat{x}+\hat{y}} + e^{i\theta} c_{\bar{r}+\hat{x}} - c_{\bar{r}+\hat{y}} + ic_{\bar{r}}$, and $D(\theta) = e^{i\theta} d_{\bar{r}+\hat{x}+\hat{y}} - ie^{i\theta} d_{\bar{r}+\hat{x}} + id_{\bar{r}+\hat{y}} - d_{\bar{r}}$. The above calculation shows that Q^- and \tilde{Q}^- sectors (and c and d particles) contribute to the Berry phase additively. Berry phases of other states including $Q_r^{+\dagger}$, etc., are calculated similarly, and similar results are obtained.

Let us consider the effects of the interactions H_{SPI} in Eq. (27), which preserve chiral symmetries and the gapless edge modes. As we mentioned in the above, ‘‘phase transition’’ between two states $|\Psi_1\rangle = \prod_{\bar{r}} (Q_{\bar{r}}^{-\dagger}) |0\rangle$ and $|\Psi_2\rangle = \prod_{\bar{r}} (\tilde{Q}_{\bar{r}}^{-\dagger}) |0\rangle$ takes place as varying values of τ_0 and τ_1 . At 1/4 filling for $\tau_0 > \tau_1 > 2\lambda (> 0)$, the ground state is given by $|\Psi_1\rangle$, and the Berry phase $\gamma_L = \pi$ as we calculated. As λ increases, the intraspecies nearest-neighbor (NN) repulsions get stronger, and at $2\lambda = \tau_0 - \tau_1$, there emerge tremendous degeneracies; i.e., states such as $|\Psi_1\rangle$, $\prod(\dots, Q_{\bar{r}-\hat{x}}^{-\dagger} \tilde{Q}_{\bar{r}}^{-\dagger} Q_{\bar{r}+\hat{x}}^{-\dagger} \dots |0\rangle$, $\prod(\dots, Q_{\bar{r}-\hat{x}}^{-\dagger} \tilde{Q}_{\bar{r}+\hat{x}}^{-\dagger} Q_{\bar{r}+\hat{x}}^{-\dagger} \dots |0\rangle$, etc., have all the same energy. Because of this degeneracy, the Berry phase is undefined. Even in this case, the gapless edge modes exist but they cannot be identified because of the tremendous degeneracy. As the intraspecies NN repulsion is getting stronger [$2\lambda > \tau_0 - \tau_1$], all cubes in one subsystem, say, even cubes, are occupied by $Q_{\bar{r}}^-$, whereas odd cubes are empty or occupied by $\tilde{Q}_{\bar{r}}^-$. The number of the empty cubes is equal to that of the doubly occupied cubes as there is no interspecies repulsion between $Q_{\bar{r}}^-$ and $\tilde{Q}_{\bar{r}}^-$. When we further add on-cube interspecies repulsion such as $\lambda' \sum (K_{\bar{r}}^- - \frac{1}{2})(\tilde{K}_{\bar{r}}^- - \frac{1}{2})$, the degeneracy is resolved. The ground state is simply doubly degenerate and has a Néel-type order, i.e., $(\dots Q_{\bar{r}-\hat{x}}^{-\dagger} \tilde{Q}_{\bar{r}}^{-\dagger} Q_{\bar{r}+\hat{x}}^{-\dagger} \tilde{Q}_{\bar{r}+2\hat{x}}^{-\dagger} \dots |0\rangle$.

In the thermodynamic limit, these two states are totally disconnected, and the Berry phase can be defined for each state as in the ordinary local order parameter such as magnetization in the Ising model. Each state has Berry phase $\gamma_L = \pi$.

In the following, we calculate Berry phases γ_L for the system with the additional interaction, H_{II} [Eq. (28)], by numerical methods. The form of interaction H_{II} does not break the inversion symmetry of Eq. (25). In general, without gap closing, the topological phase is robust for the presence of H_{II} . The interaction does not allow each particle to become the CLSs of Q^+ , Q^- , \tilde{Q}^+ , and \tilde{Q}^- since the number operators of the CLSs no longer commute the total Hamiltonian $H_{\text{SP}} + H_{\text{II}}$. The CLSs are deformed by the interactions. Along with this, by varying the value of V , the many-body gap can vanish. Hence, the interaction H_{II} can induce a topological phase transition.

In particular, we are interested in how states change as V is increased. In order to have a well-defined Berry phase, the energy gap $\Delta E(\theta)$ between the ground state and first excited states has to be positive for any $\theta \in [0, 2\pi]$. Then, we define $\Delta E \equiv \text{Min}[\Delta E(\theta)]$, and calculate it numerically. The results of γ_L and ΔE are shown in Figs. 8(a) and 8(b) for the 1/4-filling state. Data show that the Berry phase $\gamma_L = \pi$ for $V < V_c \simeq 2.7$, indicating that the state is topologically nontrivial, whereas from $V = V_c$ the Berry phase begins to be unstable and random. ΔE is also vanishingly small for $V > V_c$. Similar behavior of the Berry phase was observed in Ref. [64]. In Fig. 8(c), we also show energies of the ground state, and first and second excited states without twist. The energy gap of the ground state decreases and gradually vanishes as a function of V . This indicates that the system turns into a gapless metallic phase although the critical transition point cannot be extracted due to the finite-size effects. On the other hand, we also calculate the half-filled case, the results of γ_L , ΔE , and energies of the ground state, and first and second excited states without twist are shown in Figs. 8(d)–8(f). The Berry phase γ_L in Fig. 8(d) is stable and stays zero for $V \lesssim 2$. For $V \gtrsim 2$ it turns unstable and random since ΔE vanishes as shown in Fig. 8(e). The calculations of energies in Fig. 8(f) show that the stable ground state exists for $V < V'_c \simeq 2.0$, and apparently a gapless metallic state emerges for $V > V'_c$. The difference between the 1/4-filling and half-filling states comes from the fact that the topological nontrivial state with $\gamma_L = \pi$ is realized at the 1/4 filling, whereas the trivial state with $\gamma_L = 0 \pmod{2\pi}$ is realized at half filling.

In the above, we investigated the local quantity, the Berry phase, related to topological properties of the systems. As shown in the previous work on the Creutz ladder [34], there is a nonlocal order parameter of Z_2 topological symmetry, i.e., the string operator [65–67]. We can define a similar quantity in the present bilayer systems, which we call a Z_2 order parameter and string operator. These operators are defined in terms of the LIOMs, and for the Hamiltonian H_{SP} ,

$$Z_2 = (-1)^{\sum_{\bar{r}} (K_{\bar{r}}^+ + K_{\bar{r}}^- + \tilde{K}_{\bar{r}}^+ + \tilde{K}_{\bar{r}}^-)}. \quad (38)$$

As $K_{\bar{r}}^- = Q_{\bar{r}}^{-\dagger} Q_{\bar{r}}^-$, etc., the Z_2 operator in Eq. (38) is closely related to the Berry phase calculated in the above. Under the OBC considered in the above, the Z_2 operator tends to

$$Z_2 \rightarrow (-1)^{\sum_{n=0}^L \sum_{\bar{r}=(n,0)} (c_{\bar{r}}^\dagger c_{\bar{r}} + c_{\bar{r}+\hat{y}}^\dagger c_{\bar{r}+\hat{y}} + d_{\bar{r}}^\dagger d_{\bar{r}} + d_{\bar{r}+\hat{y}}^\dagger d_{\bar{r}+\hat{y}})},$$

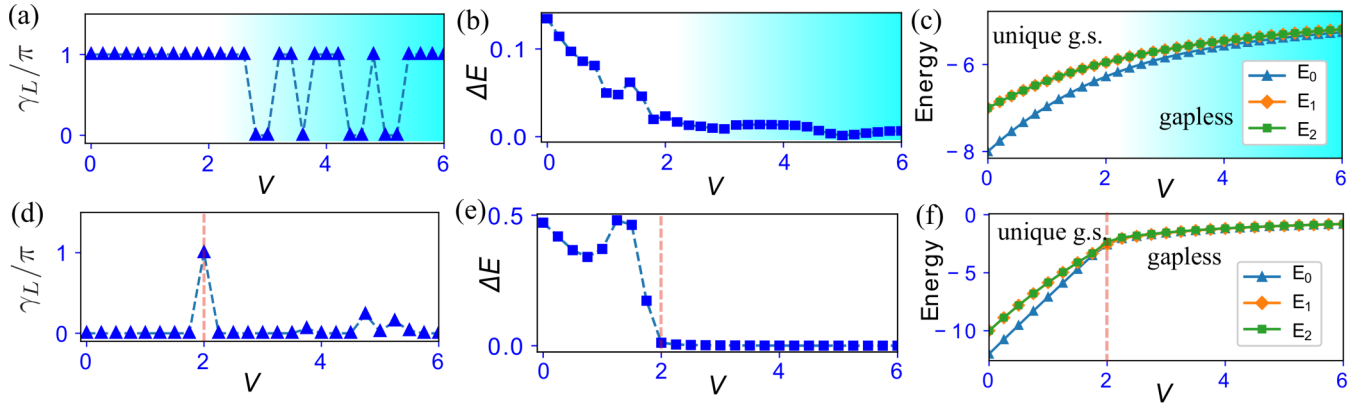


FIG. 8. (a) Berry phase γ_L as a function of V for 1/4 filling. For $V > V_c \simeq 2.7$, the Berry phase is unstable. (b) The energy gap ΔE for 1/4 filling (the difference between ground state and first excited state). Both results indicate the existence of some kind of crossover in the vicinity of V_c . (c) Energy of the ground state, and first and second excited states without twist. The energy gap of the ground state decreases as V increases, but it keeps finite even for $V > V_c$. System size $L = 4$ (4×4 sites) and 4 particles. (d) Berry phase γ_L as a function of V for half filling. For $V > V_c \simeq 2$, the Berry phase is unstable. (e) The energy gap ΔE for half filling (the difference between ground state and first excited state). Both results indicate the existence of a phase transition in the vicinity of $V_c = 2$. (f) Energy of the ground state, and first and second excited states without twist for half filling. The gapless ground state emerges for $V > V_c' \simeq 2.0$. System size $L = 4$ (4×4 sites) and 8 particles.

where we have added the terms such as $[\omega_{(0,0),\hat{y}}^{B\dagger}\omega_{(0,0),\hat{y}}^B + \tilde{\omega}_{(L,0),\hat{y}}^{A\dagger}\tilde{\omega}_{(L,0),\hat{y}}^A]$ to make $Z_2 = \pm 1$. On the other hand, for the string operator, $\mathcal{O}(\ell, m)$, we define it as follows:

$$\mathcal{O}(\ell, m) = (-1)^{\sum_{n=\ell}^m \sum_{\vec{r}=(n,0)} (K_{\vec{r}}^+ + K_{\vec{r}}^- + \tilde{K}_{\vec{r}}^+ + \tilde{K}_{\vec{r}}^-)}. \quad (39)$$

In the above, we studied the ‘‘phase transition’’ caused by the interactions. For small λ , the state has the Berry phase $\gamma_L = \pi$. In this state $|\Psi_1\rangle$, $\langle K_{\vec{r}}^- \rangle = 1$ and the other expectation values are vanishing, and therefore $\langle \mathcal{O}(\ell, m) \rangle \neq 0$. On the other hand, for $2\lambda \geq \tau_0 - \tau_1$, there exist a large number of degenerate states, in which $\langle K_{\vec{r}}^- \rangle = 0$ or 1, randomly. Therefore, the microcanonical ensemble gives $\langle \mathcal{O}(\ell, m) \rangle = 0$. By adding the on-cube interspecies repulsion, the degeneracy is resolved except for the macroscopic one, and then $\langle \mathcal{O}(\ell, m) \rangle \neq 0$. The above consideration of the various states shows that the Berry phase and the string operator give the consistent results as topological order parameters.

Finally, we study the 1/4-filling state by using partial-reflection (PR) overlap of wave functions, which was recently proposed for a detailed investigation of the SPT phase [68,69]. In general, the PR overlap is defined as

$$Z_{\text{PR}} = \langle \Psi | \mathcal{R}_{\text{PR}} | \Psi \rangle, \quad (40)$$

where \mathcal{R}_{PR} is the PR operator that reflects the sites within a segment of lattice with respect to its central link(s). Here, we consider the smallest PR segment, i.e., a single cube located at site $\vec{r} = \vec{r}_0$. Then, \mathcal{R}_{PR} operates as [69]

$$\begin{aligned} c_{\vec{r}_0} &\rightarrow ic_{\vec{r}_0+\hat{x}+\hat{y}}, & c_{\vec{r}_0+\hat{x}} &\rightarrow ic_{\vec{r}_0+\hat{y}}, \\ c_{\vec{r}_0+\hat{x}+\hat{y}} &\rightarrow ic_{\vec{r}_0}, & c_{\vec{r}_0+\hat{y}} &\rightarrow ic_{\vec{r}_0+\hat{x}}. \end{aligned} \quad (41)$$

Then, the PR overlap of the 1/4-filling ground state is obtained by calculation of the following quantity:

$$Z_{\text{PR}}^{(1)}(1/4) = \langle \Psi_1 | \mathcal{R}_{\text{PR}} | \Psi_1 \rangle. \quad (42)$$

After some analytical calculation, we obtain

$$Z_{\text{PR}}^{(1)}(1/4) = \frac{i}{2} = e^{i\pi/2}/2. \quad (43)$$

Similarly for the state $|\Psi_2\rangle$,

$$Z_{\text{PR}}^{(2)}(1/4) = -\frac{i}{2} = e^{-i\pi/2}/2. \quad (44)$$

The above results of $Z_{\text{PR}}(1/4)$ indicates that the 1/4-filling state has Z_4 topological phase corresponding to the phase $\pi/2 = (2\pi)/4$, and a single complex fermion emerges per each boundary in the OBC by the denominator 2 [69]. The complex fermion, say, at the right boundary, is given by $(-\omega_{x=L,\hat{y}}^B - i\tilde{\omega}_{x=L,\hat{y}}^A)^\dagger$ coming from $(Q_{\vec{r}=(L,0)}^-)^\dagger$. We think that the emergent Z_4 topological phase (not Z topological phase dictated by BDI class) comes from the four flat-bands structure of the Hamiltonian H_{SP} as shown in Fig. 5. This point will be discussed further in Sec. VI.

VI. DISCUSSION AND CONCLUSION

In this paper, by making use of the cube operators, which were heuristically found as an extension of the ℓ -bits (CLS) in the Creutz ladder, we constructed bilayer flat-band Hamiltonians of the exact projective form. The models have extensive numbers of the LIOMs, and thus, full localization occurs in the bulk. Since we constructed the Hamiltonians by imposing certain symmetries, time-reversal and chiral symmetries, the constructed bilayer flat-band Hamiltonians naturally belong to a symmetric topological class in a tenfold way. In this work, we explicitly showed that the constructed bilayer flat-band Hamiltonians belong to the BDI class. From this classification, the constructed bilayer flat-band Hamiltonians exhibit some topological character, i.e., nontrivial bulk topology and presence of the gapless edge modes, in particular in one dimension. The model constructed on a quasi-1D lattice (prism lattice) explicitly exhibits SPT phase characterized by

topological indices for a periodic system, and also the existence of gapless edge modes for the open boundary. This is just bulk-edge correspondence in the complete flat-band system.

Here, we would like to give a brief discussion on topological properties of *strongly localized states*. For the Hamiltonian H_{SP} , the PR overlap shows the existence of the Z_4 topology. It is well known that Z topology of the BDI class by the topological classification actually reduces to Z_8 [70,71]. For H_{SP} , the Z_4 topology seems quite plausible as the system has four flat-band structure. Not only in prism lattices but also in thin cylinder lattices, gapless edge modes are discovered relying on the form of the cube operators. By the topological classification, 2D systems in the BDI class have no bulk topological properties. We think that the above results come from the fact that the localized states in the present models are all described by the ℓ -bits, and are strictly confined in a single cube. Therefore, the spatial dimension does not seem

relevant for topological classification in the present systems. In fact, a close look at the one-dimensional edge modes appearing in the thin cylinder bilayer system reveals that the edge modes \mathcal{B}_C 's are composed of edges modes in the the quasi-1D Hamiltonian similar to H_{SP} located in the y direction (see Fig. 6). The chiral symmetry $\mathcal{S}_x K$ plays an important role for lacing edge modes in the Hamiltonian H_{SP} along the x direction. This is the mechanism for the emergence of the one-dimensional edge modes; that is, topological properties of the Hamiltonian H_{SP} and the chiral symmetry collaborate. Anyway, careful investigation is required to clarify if this kind of phenomenon is generic or specific. This is a future work.

ACKNOWLEDGMENT

The work is supported in part by JSPS KAKENHI Grant No. JP21K13849 (Y.K.).

-
- [1] A. Smith, J. Knolle, D. L. Kovrizhin, and R. Moessner, *Phys. Rev. Lett.* **118**, 266601 (2017).
- [2] A. Smith, J. Knolle, R. Moessner, and D. L. Kovrizhin, *Phys. Rev. Lett.* **119**, 176601 (2017).
- [3] M. Schulz, C. A. Hooley, R. Moessner, and F. Pollmann, *Phys. Rev. Lett.* **122**, 040606 (2019).
- [4] S. Scherg, T. Kohlert, P. Sala, F. Pollmann, H. M. Bharath, I. Bloch, and M. Aidelsburger, *arXiv:2010.12965*.
- [5] P. A. McClarty, M. Haque, A. Sen, and J. Richter, *Phys. Rev. B* **102**, 224303 (2020).
- [6] R. Nandkishore and D. A. Huse, *Annu. Rev. Condens. Matter Phys.* **6**, 15 (2015).
- [7] D. A. Abanin, E. Altman, I. Bloch, and M. Serbyn, *Rev. Mod. Phys.* **91**, 021001 (2019).
- [8] J. Z. Imbrie, V. Ros, and A. Scardicchio, *Ann. Phys.* **529**, 1600278 (2017).
- [9] M. Serbyn, Z. Papić, and D. A. Abanin, *Phys. Rev. Lett.* **111**, 127201 (2013).
- [10] S. Mukherjee, M. Di Liberto, P. Öhberg, R. R. Thomson, and N. Goldman, *Phys. Rev. Lett.* **121**, 075502 (2018).
- [11] J. Vidal, R. Mosseri, and B. Douçot, *Phys. Rev. Lett.* **81**, 5888 (1998).
- [12] C. Naud, G. Faini, and D. Mailly, *Phys. Rev. Lett.* **86**, 5104 (2001).
- [13] J. H. Bardarson, F. Pollmann, and J. E. Moore, *Phys. Rev. Lett.* **109**, 017202 (2012).
- [14] S. Flach, D. Leykam, J. D. Bodyfelt, P. Matthies, and A. S. Desyatnikov, *Europhys. Lett.* **105**, 30001 (2014).
- [15] T. Mizoguchi and Y. Hatsugai, *Europhys. Lett.* **127**, 47001 (2019).
- [16] Y. Kuno, T. Mizoguchi, and Y. Hatsugai, *Phys. Rev. B* **102**, 241115(R) (2020).
- [17] Y. Kuno, T. Mizoguchi, and Y. Hatsugai, *Phys. Rev. A* **102**, 063325 (2020).
- [18] N. Regnault and B. A. Bernevig, *Phys. Rev. X* **1**, 021014 (2011).
- [19] E. J. Bergholtz and Z. Liu, *Int. J. Mod. Phys. B* **27**, 1330017 (2013).
- [20] H. Guo, S. Q. Shen, and S. Feng, *Phys. Rev. B* **86**, 085124 (2012).
- [21] J. C. Budich and E. Ardonne, *Phys. Rev. B* **88**, 035139 (2013).
- [22] S. Barbarino, D. Rossini, M. Rizzi, M. Fazio, G. E. Santoro, and M. Dalmonte, *New J. Phys.* **21**, 043048 (2019).
- [23] P. Tomczak and J. Richter, *J. Phys. A: Math. Gen.* **36**, 5399 (2003).
- [24] J. Richter, J. Schulenburg, P. Tomczak, and D. Schmalfuß, *Condens. Matter Phys.* **12**, 507 (2009).
- [25] O. Derzhko and J. Richter, *Eur. Phys. J. B* **52**, 23 (2006).
- [26] J. Wildeboer and A. Seidel, *Phys. Rev. B* **83**, 184430 (2011).
- [27] W. Jiang, D. J. P. de Sousa, J.-P. Wang, and T. Low, *Phys. Rev. Lett.* **126**, 106601 (2021).
- [28] W. Jiang, X. Ni, and F. Liu, *Acc. Chem. Res.* **54**, 416 (2021).
- [29] W. Jiang, Z. Liu, J.-W. Mei, B. Cui, and F. Liu, *Nanoscale* **11**, 955 (2019).
- [30] M. Creutz, *Phys. Rev. Lett.* **83**, 2636 (1999).
- [31] C. Danieli, A. Andreanov, and S. Flach, *Phys. Rev. B* **102**, 041116(R) (2020).
- [32] N. Roy, A. Ramachandran, and A. Sharma, *Phys. Rev. Res.* **2**, 043395 (2020).
- [33] Y. Kuno, T. Orito, and I. Ichinose, *New J. Phys.* **22**, 013032 (2020).
- [34] T. Orito, Y. Kuno, and I. Ichinose, *Phys. Rev. B* **101**, 224308 (2020).
- [35] T. Orito, Y. Kuno, and I. Ichinose, *Phys. Rev. B* **103**, L060301 (2021).
- [36] A. Bermudez, D. Patanè, L. Amico, and M. A. Martin-Delgado, *Phys. Rev. Lett.* **102**, 135702 (2009).
- [37] J. Jünemann, A. Piga, S.-J. Ran, M. Lewenstein, M. Rizzi, and A. Bermudez, *Phys. Rev. X* **7**, 031057 (2017).
- [38] N. Sun and L.-K. Lim, *Phys. Rev. B* **96**, 035139 (2017).
- [39] J. Zurita, C. E. Creffield, and G. Platero, *Adv. Quantum Technol.* **3**, 1900105 (2020).
- [40] Y. Kuno, *Phys. Rev. B* **101**, 184112 (2020).
- [41] C. K. Chiu, J. C. Y. Teo, A. P. Schnyder, and S. Ryu, *Rev. Mod. Phys.* **88**, 035005 (2016).
- [42] A. W. W. Ludwig, *Phys. Scr.* **T168**, 014001 (2016).

- [43] A. Altland and M. R. Zirnbauer, *Phys. Rev. B* **55**, 1142 (1997).
- [44] S. Ryu, A. P. Schyder, A. Furusaki, and A. W. W. Ludwig, *New J. Phys.* **12**, 065010 (2010).
- [45] F. Pollmann, A. M. Turner, E. Berg, and M. Oshikawa, *Phys. Rev. B* **81**, 064439 (2010).
- [46] X. Chen, Z.-C. Gu, and X.-G. Wen, *Phys. Rev. B* **84**, 235128 (2011).
- [47] F. Pollmann, E. Berg, A. M. Turner, and M. Oshikawa, *Phys. Rev. B* **85**, 075125 (2012).
- [48] Y. Bahri, R. Vosk, E. Altman, and A. Vishwanath, *Nat. Commun.* **6**, 7341 (2015).
- [49] S. Sachdev and J. Ye, *Phys. Rev. Lett.* **70**, 3339 (1993).
- [50] S. Sachdev, *Phys. Rev. X* **5**, 041025 (2015).
- [51] A. Kitaev, talk at KITP Program: Entanglement in Strongly-Correlated Quantum Matter, 2015 (unpublished).
- [52] J. K. Asboth, L. Oroszlany, and A. Palyi, *A Short Course on Topological Insulators: Band-Structure Topology and Edge States in One and Two Dimensions* (Springer, Berlin, 2016).
- [53] J. Zak, *Phys. Rev.* **134**, A1602 (1964).
- [54] J. Zak, *Phys. Rev.* **134**, A1607 (1964).
- [55] C. Fang, M. J. Gilbert, and B. A. Bernevig, *Phys. Rev. B* **86**, 115112 (2012).
- [56] Y.-Z. You, A. W. W. Ludwig, and C. Xu, *Phys. Rev. B* **95**, 115150 (2017).
- [57] We employed the Quspin solver: P. Weinberg and M. Bukov, *SciPost Phys.* **7**, 20 (2019); **2**, 003 (2017).
- [58] Y. Hatsugai, *J. Phys. Soc. Jpn.* **74**, 1374 (2005).
- [59] Y. Hatsugai, *J. Phys. Soc. Jpn.* **75**, 123601 (2006).
- [60] Y. Hatsugai, *J. Phys. Condens. Matter* **19**, 145209 (2007).
- [61] T. Hirano, H. Katsura, and Y. Hatsugai, *Phys. Rev. B* **77**, 094431 (2008).
- [62] H. Katsura, T. Hirano, and Y. Hatsugai, *Phys. Rev. B* **76**, 012401 (2007).
- [63] Y. Hatsugai and I. Maruyama, *Europhys. Lett.* **95**, 20003 (2011).
- [64] H. Guo, *Phys. Rev. A* **86**, 055604 (2012).
- [65] A. Y. Kitaev, *Phys. Usp.* **44**, 131 (2001).
- [66] P. Fendley, *J. Stat. Mech.: Theory Exp.* (2012) P11020.
- [67] M. McGinley, J. Knolle, and A. Nunnenkamp, *Phys. Rev. B* **96**, 241113(R) (2017).
- [68] F. Pollmann and A. M. Turner, *Phys. Rev. B* **86**, 125441 (2012).
- [69] H. Shapourian, K. Shiozaki, and S. Ryu, *Phys. Rev. Lett.* **118**, 216402 (2017).
- [70] L. Fidkowski and A. Kitaev, *Phys. Rev. B* **81**, 134509 (2010).
- [71] L. Fidkowski and A. Kitaev, *Phys. Rev. B* **83**, 075103 (2011).